RSC Chemical Biology

ROYAL SOCIETY OF CHEMISTRY

PAPER

View Article Online
View Journal | View Issue

Cite this: *RSC Chem. Biol.*, 2022, 3, 895

Landscaping macrocyclic peptides: stapling hDM2-binding peptides for helicity, protein affinity, proteolytic stability and cell uptake†

Aline D. de Araujo, Junxian Lim, Kai-Chen Wu, Huy N. Hoang, Huy T. Nguyen and David P. Fairlie *

Cyclic peptides that modulate protein–protein interactions can be valuable therapeutic candidates if they can be delivered intact to their target proteins in cells. Here we systematically compare the effects of different helix-inducing cyclization constraints on the capacity of a macrocyclic peptide component to confer α-helicity, protein-binding affinity, resistance to degradative proteases and cell uptake to a 12-residue peptide fragment of tumor suppressor protein p53. We varied the helix-inducing constraint (hydrocarbon, lactam, aliphatic or aromatic thioether, *etc.*) and the position of the cyclization linker (*i* to *i* + 4 or *i* to *i* + 7 bridges) in order to sculpt the macrocyclic size, stabilize its structure, and promote cell uptake. We find that rigidifying the macrocycle leads to higher alpha helicity, target affinity and proteolytic stability to different extents, whereas cell uptake of compounds shown here is mostly driven by hydrophobicity and aromaticity of the macrocycle.

Received 1st December 2021,
Accepted 19th May 2022

DOI: 10.1039/d1cb00231g

rsc.li/rsc-chembio

Introduction

Protein–protein interactions (PPIs) control most cellular processes, but their dysregulation can lead to disease. Finding ways to activate or inhibit PPIs is important for design of future therapeutics.[1] Most PPIs involve large, shallow, and highly polar interacting surfaces (1500–3000 Å^2).[2] These present significant challenges for binding conventional small molecule drugs that require small hydrophobic binding pockets in proteins.[1] PPIs are often mediated by helical motifs, comprising 1–4 α-helical turns (4–15 amino acids).[3–6] Synthetic peptides corresponding to such helical regions of proteins are attractive leads for drug design.[3–6] However, in water outside proteins these peptides are not thermodynamically stable α-helices, raising the entropic penalty for target binding. They are also usually too polar to enter cells where most PPIs are located. To address these limitations, two residues on the same face of a putative peptide helix may be covalently crosslinked ('stapled'), for example by lactamization,[3] olefin ring-closing metathesis (RCM),[5,6] cysteine thiolation[7] or 1,3-dipolar cycloaddition[8] (Fig. 1), to form a macrocyclic component that may stabilize a peptide helix. Incorporating such crosslinks can also potentially alter aqueous *versus* membrane solubility, enhance chemical and metabolic stability, and increase cell uptake and bioavailability.[3–9]

A remarkable feature of some peptides with hydrocarbon-linked macrocyclic components is their ability to enter cells and bind to intracellular proteins.[6] Their membrane permeability may be due to extended hydrophobicity introduced by the

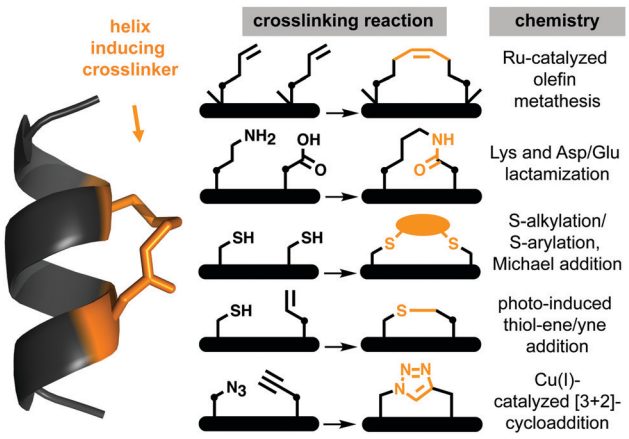

Fig. 1 Chemical macrocyclization strategies to stabilize short peptide sequences into helices *via* side-chain crosslinking. The stapling constraints are usually imposed between (*i* → *i* + 4)- (pictured) or (*i* → *i* + 7)-positions within the peptide. • means $(CH_2)_n$, *n* = 0, 1, 2,….

Division of Chemistry and Structural Biology, ARC Centre of Excellence for Innovations in Peptide and Protein Science, Institute for Molecular Bioscience, The University of Queensland, Brisbane, QLD 4072, Australia.
E-mail: d.fairlie@uq.edu.au

† Electronic supplementary information (ESI) available: Syntheses, chemical, structural and biological characterisation data. Experimental procedures for compound syntheses, characterization by HPLC and MS analysis, hDM2 binding assays, proteolysis analysis and cell-based assays (PDF). See DOI: **https://doi.org/10.1039/d1cb00231g**

linker, facilitating interaction with phospholipid membranes. However, increasing hydrophobicity too much may lead to aggregation or cell lysis. Moreover, hydrophobicity is arguably not the sole contributor to cell uptake, with amphipathicity, charge, dipole and helicity also potentially contributing to endocytosis and release into the cytosol.[10,11]

Systematic studies show that a specific lactam bridge across five residues ($i \rightarrow i + 4$) is more α-helix inducing than hydrocarbon, cysteinyl and triazole linkers in cyclic pentapeptides alone[12] or in 10–20 residue peptides.[12,13] Others found that lactam and hydrocarbon linkers at the centre of a specific 12-mer peptide induced comparable helicity.[14] Positioning an ($i \rightarrow i + 4$) hydrocarbon linker in a BCL-2 binding peptide with positive charges led to increased helicity and cell uptake only when positioned at the amphipathic boundary.[10] Fewer ($i \rightarrow i + 7$) crosslinkers[15,16] have been comparatively investigated for their effects on biophysical properties of peptides.

Here we systematically evaluate the impact of ($i \rightarrow i + 4$) and ($i \rightarrow i + 7$) crosslinkers of varying composition, hydrophobicity and flexibility, on structural and biophysical properties of a bioactive peptide, Ac-LTFEHYWAQLTS-$CONH_2$ (**1**).[17] Discovered by phage display, this peptide inhibits interaction of tumor suppressor protein p53 with hDM2, a protein that prevents p53 action and transports it from nucleus to cytosol. hDM2 is also a ligase that attaches ubiquitin covalently to p53, marking it for proteasomal degradation. Compounds that bind to hDM2 can reactivate the p53 pathway for cell-cycle arrest and apoptosis of tumor cells.[18] However, this peptide is prone to proteolytic degradation and unable to cross cell membranes, prompting studies on increasing its stability and cell uptake.[19–21] Here we focus on comparing hydrocarbon, thioether, triazole and lactam linkers in **1** for their ability to increase α-helicity, hDM2 affinity, resistance to proteases, and cell uptake without cell lysis.

Results

To incorporate helix-inducing cyclic constraints into the peptide, we were careful to retain essential hDM2-binding residues (Phe3, Trp7, Leu10) but replaced His5 with Glu5 to improve solubility without affecting binding to hDM2.[19] To measure cell uptake, the N-terminal acetyl group was replaced by β-alanine linked to fluorescein (FITC). We investigated effects of different cyclic components on α-helicity (measured by circular dichroism (CD) spectra in aqueous media), binding affinity for hDM2 (measured by competition for hDM2 binding of FITC-labelled **1** using fluorescence polarization (FP) assays), and proteolytic stability (using LCMS after incubation with chymotrypsin, pepsin or proteinase K). Later we describe their hydrophobicity and propensity for cell uptake and cell lysis.

($i \rightarrow i + 4$)-crosslinkers

Positions 4 and 8 in **1** were stapled (Fig. 2A) with a hydrocarbon linker[5] (**2a**), a Lys-Asp lactam bridge[3] (**2b**), a *para*-benzyl bis-thioether linker[22] (**2c**), a perfluorophenyl bis-thioether[23] (**2d**) or its homocysteine variant (**2e**).[24] Since the lactam bridge is known to be the most effective helix inducer from the C-terminus,[13] we included analogue **2f** (Fig. 2A). We also synthesized bicyclic **2g** and **2h**, since two bridges (two lactams or one hydrocarbon/one lactam) can strongly enforce α-helicity,[13,25] the hydrocarbon creating a larger hydrophobic surface to assist membrane interaction.

Peptides **2a** and **2e** induced ~60% helicity in aqueous phosphate buffer (10 mM, pH 7.4) (Fig. 2B), with the lactam linkage conferring greater helicity from the C-terminus (**2f**). Thioether **2c** had much less helicity than **2a**. Compound **2d** gave a distorted CD curve, possibly obscured by strong absorbance from the fluoroaryl moiety,[23,24] but not for **2e** that had some helix-like ellipticity despite a perfluoroaryl crosslink. Adding a second helix-inducing constraint into **2f**, either a second lactam (**2g**) or hydrocarbon (**2h**), enhanced helicity (~90%) independent of solvent (Fig. 2C), consistent with other findings.[3a,13,26] Only small variations in helicity (±12%) were observed in CD spectra for **1** or **2a–h** in 10 mM phosphate buffer, 20% acetonitrile in water or 20 mM SDS buffer (sodium dodecyl sulfate, 10 mM sodium phosphate, 0.15 M NaF buffer pH 7.4) (Fig. 2C). Enhanced α-helicity did not correlate with binding affinity for hDM2, as determined by competitive binding with **1-FITC** to hDM2 (Fig. 2D). Only lactam peptides **2b**, **2f**, **2g** had higher affinity than **1**. The N-terminal hydrocarbon cycle in **2h** had reduced binding affinity for hDM2.

Stapling protected against proteolysis (Fig. 2E) compared to unstapled **1** that was cleaved within 1 h by chymotrypsin, pepsin or proteinase K at positions 3–4, 6–7, 10–11, 11–12. Hydrocarbon or lactam stapling (**2a**, **2b**, **2g**, **2h**) maintained peptides intact, cleavage only occurring in **2f** outside the cycle at the distant 3–4 position, whereas thioethers **2c–e** were not fully protected (Fig. 2E), with positions outside and inside the cycle vulnerable to cleavage. Results are consistent with constrained α-helices[26a,27d,27d] not being flexible enough to present the extended β-strand conformation required for substrate cleavage by proteases.[27]

Aliphatic ($i \rightarrow i + 7$)-crosslinkers

The prototype of this series has an α-methylated 11-membered alkene tether[5] between positions 4 and 11 (**3a**, Fig. 3A) and was developed into an anticancer drug candidate.[19] Alternatively, cysteines may be linked with aliphatic crosslinkers using thiol–ene photochemistry,[15] thiolation under high temperature and base[28] or with Zn^{2+} salts,[29] or *via* selenocysteine stapling.[16] Here we use $Zn(OAc)_2$-assisted thiolation with dibromooctane[29] to make ($i \rightarrow i + 7$) thioethers **3b–e** (Fig. 3A), with cysteines (L-Cys4/L-Cys11, **3b**; D-Cys4/L-Cys11, **3c**) or α-methyl cysteines (L-(αMe) Cys4/L-(αMe)Cys11, **3d**; D-(αMe)Cys4/L-(αMe)Cys11, **3e**).

In aqueous buffer, **3b** did not show a CD spectrum typical of an α-helix (Fig. S2, ESI†), possibly due to aggregation, while **3c** showed some helicity (38%, Fig. 3B). The α-methyl groups in **3d** and **3e** increased helicity to 70% (Fig. 3B). The α-methylated **3a** also had higher helicity (57%) than non-αMe analogues. Helicity was greater in the presence of SDS micelles (Fig. 3C). However, helicity did not correlate with binding affinity for hDM2 (Fig. 3C and D), suggesting that some degree of induced fit occurs on binding to this protein, with all five analogues having

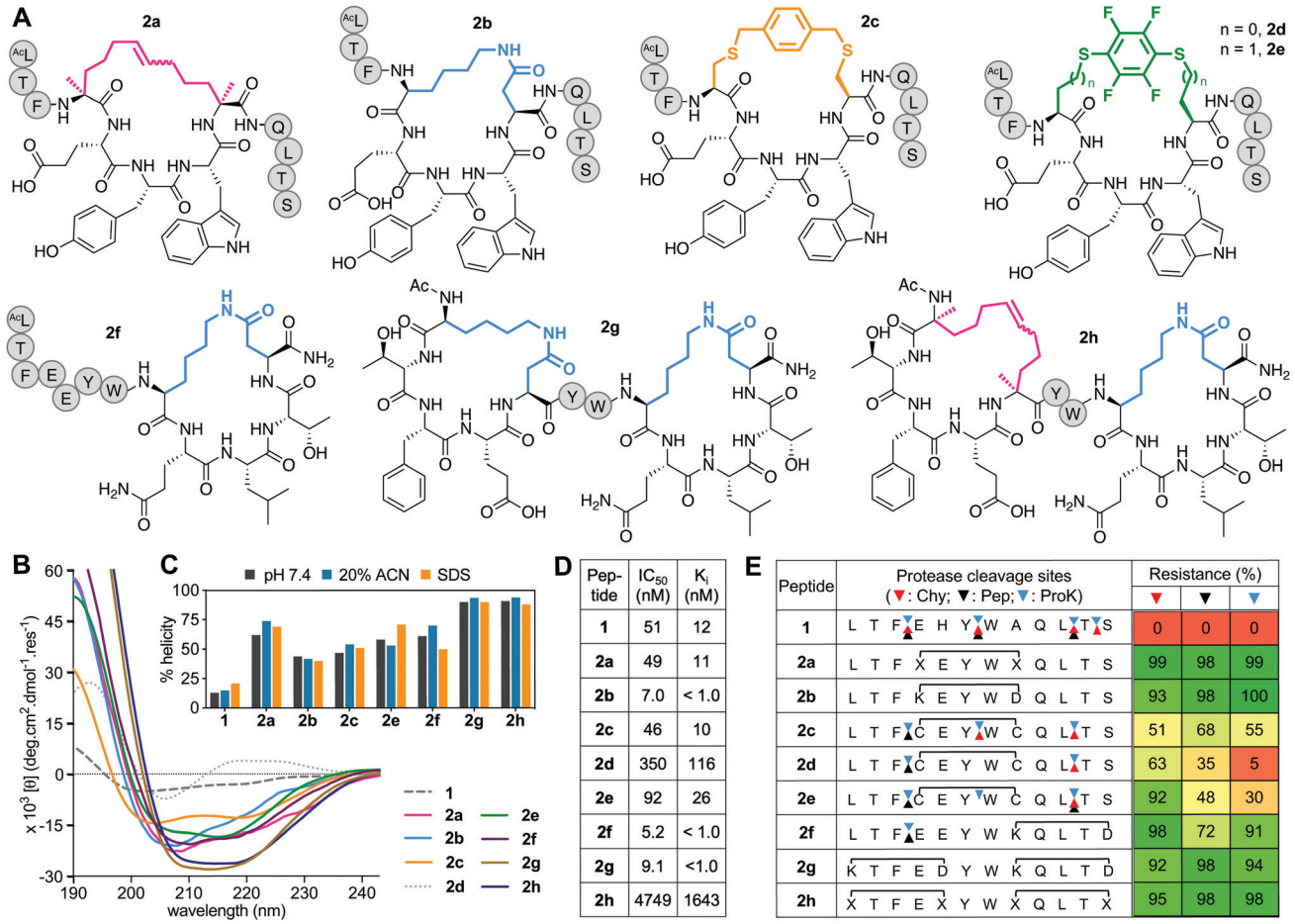

Peptide	IC_{50} (nM)	K_i (nM)
1	51	12
2a	49	11
2b	7.0	< 1.0
2c	46	10
2d	350	116
2e	92	26
2f	5.2	< 1.0
2g	9.1	<1.0
2h	4749	1643

Peptide	Protease cleavage sites (▼: Chy; ▼: Pep; ▼: ProK)	Resistance (%) ▼	▼	▼
1	L T F E H Y W A Q L T S	0	0	0
2a	L T F X E Y W X Q L T S	99	98	99
2b	L T F K E Y W D Q L T S	93	98	100
2c	L T F C E Y W C Q L T S	51	68	55
2d	L T F C E Y W C Q L T S	63	35	5
2e	L T F C E Y W C Q L T S	92	48	30
2f	L T F E E Y W K Q L T D	98	72	91
2g	K T F E D Y W K Q L T D	92	98	94
2h	X T F E X Y W X Q L T X	95	98	98

Fig. 2 A. Structures of ($i \rightarrow i + 4$)-crosslinked peptides **2a–h**. B. CD spectra for **2a–h** *vs.* **1** (50 μM) in 10 mM phosphate buffer (pH 7.4) at 22 °C. C. Percent helicity calculated from CD spectra (θ_{220}) in 10 mM phosphate buffer (pH 7.4), 20% ACN or 20 mM SDS buffer. D. IC_{50} = mean peptide concentration for inhibiting 50% binding of **1-FITC** (10 nM) to hDM2 (25 nM) measured by FP. $pIC_{50} \pm$ SEM values are reported in Fig. S1 (ESI†). Binding affinity (K_i) calculated from IC_{50} values. E. Heatmap indicating percent peptide intact after 2 h incubation with chymotrypsin (Chy), pepsin (Pep) or proteinase K (ProK) at 22 °C at pH 8 or 2 (Pep only), measured by LCMS. Arrows point to respective cleavage sites as revealed by LCMS analysis of the cleaved fragments.

high affinity but α-methylation offering no enhanced binding. Further, altering the length of the aliphatic linker in **3b** by one methylene or introducing an *E*- or *Z*-alkene at a central position in the linker, did not significantly impact helicity (in 20% acetonitrile) or hDM2 affinity of the thioether.[29]

The D- or L-configuration and α-methyl modifications had more impact on stability to proteases (Fig. 3E). Upon cyclization, positions 6–7 and 10–11 inside the macrocycle became significantly protected against cleavage, but not entirely in the case of **3b**, perhaps because of its non-helical structure in aqueous buffer (Fig. 3E and Fig. S2, ESI†). Cyclization did shelter position 11–12 from degradation except to proteinase K. D-Cys at position 4 prevented proteolysis (**3c**), whereas α-methylation fully protected neighbouring positions from cleavage by all enzymes.

Aromatic ($i \rightarrow i + 7$)-crosslinkers

This series includes the benzyl bistriazole-linked peptide **4a**, *via* a two-component construction based on a triazole-stapling approach,[8] and four variants of a biphenyl-crosslinked bisthioether macrocycle **4b** (Fig. 4A), with a ($i \rightarrow i + 7$)-cysteine staple previously reported[21] with altered L- and D-Cys or αMeCys residues at the crosslinking site (**4b–e**). Peptide **4a** showed similar binding to hDM2 as previous aliphatic ($i \rightarrow i + 7$)-crosslinked counterparts, but had reduced helix induction (27%, Fig. 4B and C). Despite unnatural amino acids at stapling sites, **4a** was partially vulnerable to cleavage by proteinase K and completely cleaved by pepsin (acidic pH required for pepsin activity led to triazole protonation and destabilization) (Fig. 4E). Compound **4b** was highly helical (72%) in water but did not have higher hDM2 affinity. Incorporating α-methylation into **4b** at the Cys stapling site to form **4d** did not increase helicity or affinity but did confer strong resistance to protease degradation (Fig. 4E). Compound **4c** was the least α-helical (24%), as D-residues disrupt helix propensity, but helicity was increased by α-methylation at cysteine (64% in **4e**) without much impact on hDM2 affinity, and protected positions 3–4 and 11–12 against proteolysis (Fig. 4E), as for the previous series.

Perfluorobiphenyl ($i \rightarrow i + 7$)-crosslinkers

Incorporating perfluorobiaryl linkers to form cyclic peptides was first demonstrated by S_N-arylation of cysteine sidechains

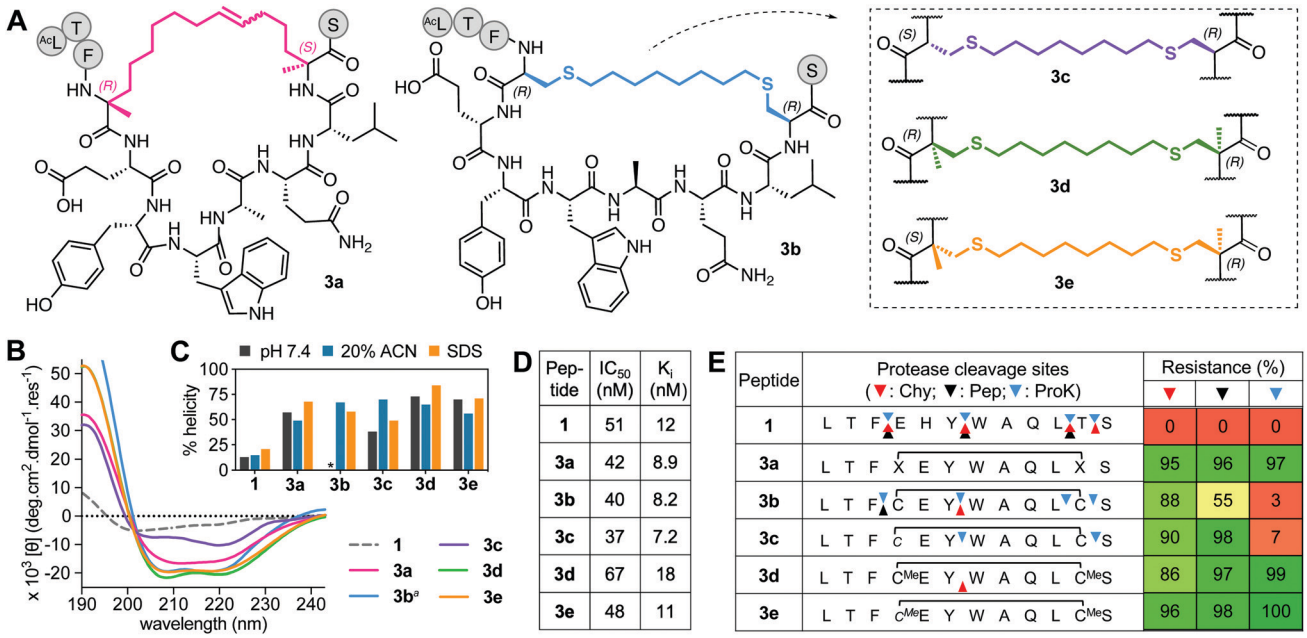

D

Peptide	IC_{50} (nM)	K_i (nM)
1	51	12
3a	42	8.9
3b	40	8.2
3c	37	7.2
3d	67	18
3e	48	11

E

Peptide	Protease cleavage sites (▼: Chy; ▼: Pep; ▼: ProK)	Resistance (%) ▼	▼	▼
1	L T F E H Y W A Q L T S	0	0	0
3a	L T F X E Y W A Q L X S	95	96	97
3b	L T F C E Y W A Q L C S	88	55	3
3c	L T F c E Y W A Q L C S	90	98	7
3d	L T F C^{Me}E Y W A Q L C^{Me}S	86	97	99
3e	L T F c^{Me}E Y W A Q L C^{Me}S	96	98	100

Fig. 3 A. Structures of aliphatic ($i \rightarrow i + 7$)-crosslinked peptides **3a–e**. B. CD spectra for **3a–e** *vs.* **1** (50 μM) in 10 mM phosphate buffer (pH 7.4, 22 °C) except **3b**[a] in 20% ACN. C. Percent helicity calculated from CD spectra (θ_{220}) in 10 mM phosphate buffer, 20% ACN or 20 mM SDS buffer (* not helical). D. IC_{50} is mean peptide concentration to inhibit 50% binding of **1-FITC** (10 nM) to hDM2 (25 nM) measured by FP. $pIC_{50} \pm$ SEM values are reported in Fig. S1 (ESI†). Binding affinity (K_i) calculated from IC_{50} values. E. Heatmap indicating percent peptide intact after 2 h incubation with chymotrypsin (Chy), pepsin (Pep) or proteinase K (ProK) at 22 °C and pH 8 or 2 (Pep only), measured by LCMS. Arrows point to respective cleavage sites as revealed by LCMS analysis of the cleaved fragments.

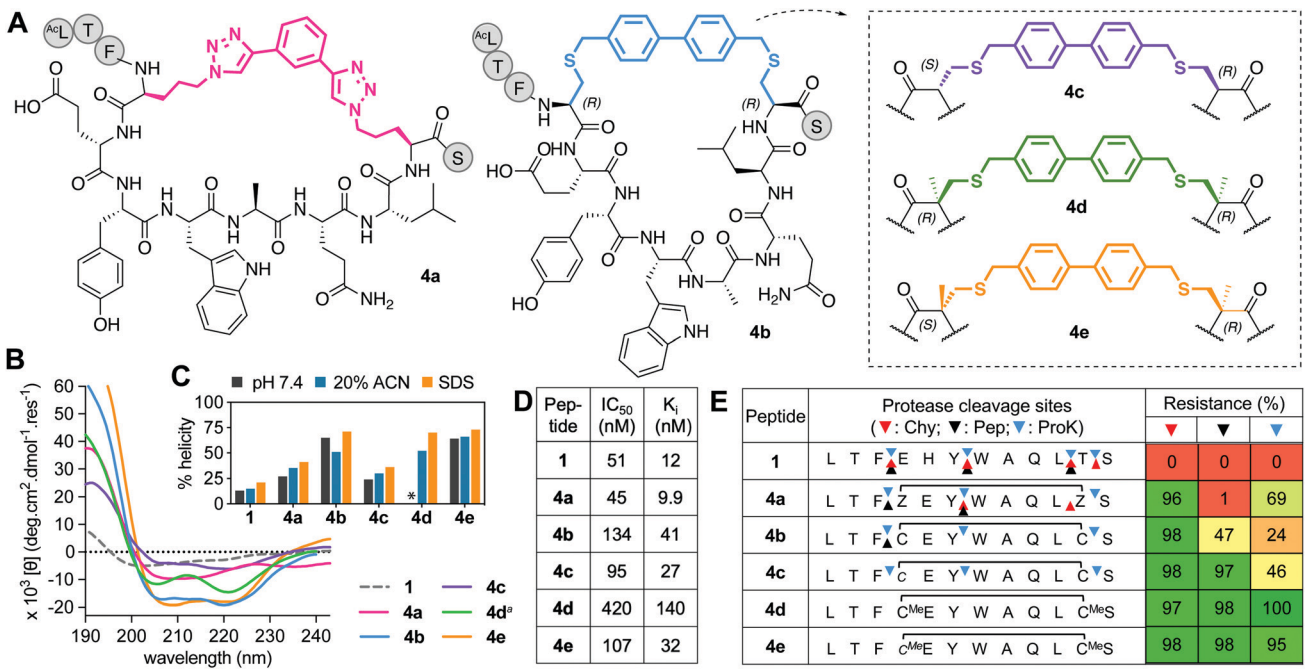

D

Peptide	IC_{50} (nM)	K_i (nM)
1	51	12
4a	45	9.9
4b	134	41
4c	95	27
4d	420	140
4e	107	32

E

Peptide	Protease cleavage sites (▼: Chy; ▼: Pep; ▼: ProK)	Resistance (%) ▼	▼	▼
1	L T F E H Y W A Q L T S	0	0	0
4a	L T F Z E Y W A Q L Z S	96	1	69
4b	L T F C E Y W A Q L C S	98	47	24
4c	L T F c E Y W A Q L C S	98	97	46
4d	L T F C^{Me}E Y W A Q L C^{Me}S	97	98	100
4e	L T F c^{Me}E Y W A Q L C^{Me}S	98	98	95

Fig. 4 A. Structures of aromatic ($i \rightarrow i + 7$)-crosslinked peptides **4a–e**. B. CD spectra for **4a–e** *vs.* **1** (50 μM) in 10 mM phosphate buffer (pH 7.4, 22 °C), except **4d**[a] in 20% ACN. C. Percent helicity calculated from CD spectra (θ_{220}) in 10 mM phosphate buffer, 20% ACN or 20 mM SDS buffer (* not helical, Fig. S2, ESI†). D. IC_{50} = mean peptide concentration to inhibit 50% binding of **1-FITC** (10 nM) to hDM2 (25 nM) measured by FP. pIC50 ± SEM values are reported in Fig. S1, ESI.† Binding affinity (K_i) calculated from IC_{50} values. E. Heatmap indicating percent peptide intact after 2 h incubation with chymotrypsin (Chy), pepsin (Pep) or proteinase K (ProK) at 22 °C at pH 8 or 2 (Pep only), measured by LCMS. Arrows show cleavage sites revealed by LCMS of the cleaved fragments.

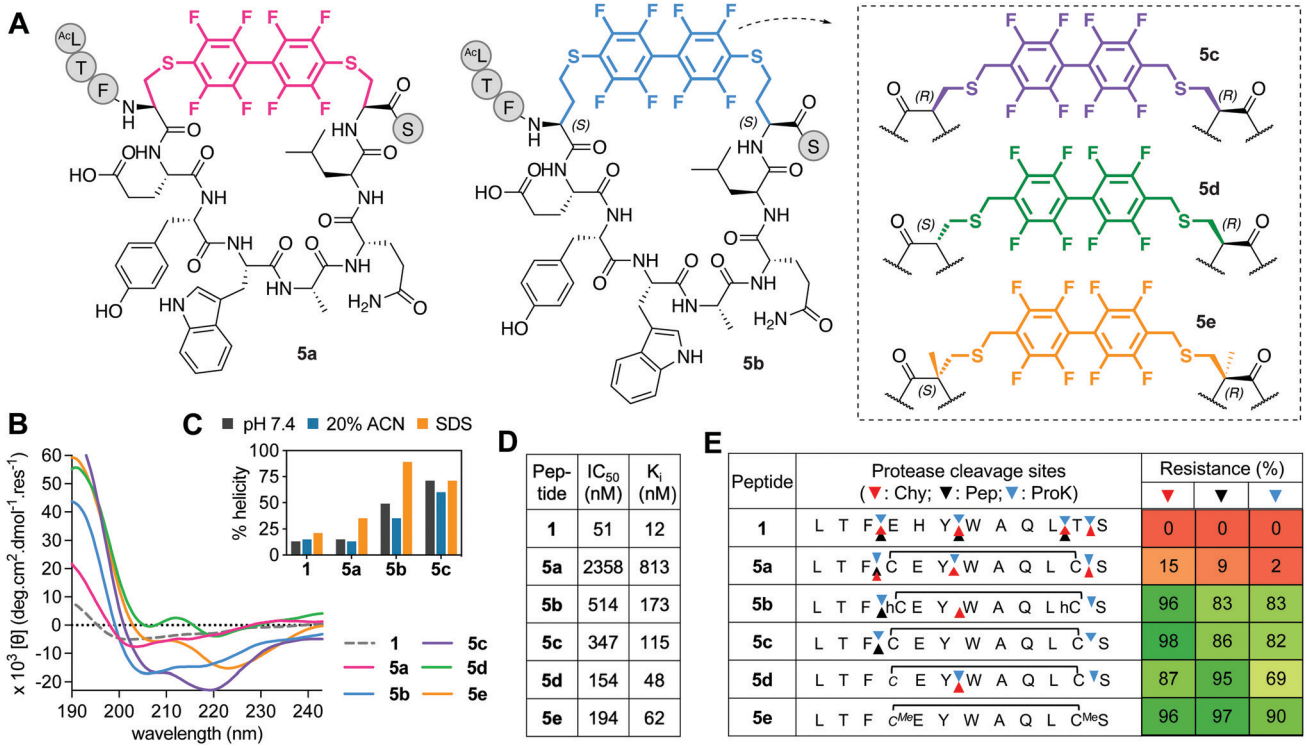

Pep-tide	IC_{50} (nM)	K_i (nM)
1	51	12
5a	2358	813
5b	514	173
5c	347	115
5d	154	48
5e	194	62

Peptide	Protease cleavage sites (▼: Chy; ▼: Pep; ▼: ProK)	Resistance (%) ▼	▼	▼
1	L T F E H Y W A Q L T S	0	0	0
5a	L T F C E Y W A Q L C S	15	9	2
5b	L T F hC E Y W A Q L hC S	96	83	83
5c	L T F C E Y W A Q L C S	98	86	82
5d	L T F C E Y W A Q L C S	87	95	69
5e	L T F C^{Me} E Y W A Q L C^{Me} S	96	97	90

Fig. 5 A. Structures of perfluorobiphenyl ($i \rightarrow i + 7$)-crosslinked peptides **5a-e.** B. CD spectra for **5a–e** *vs.* **1** (50 μM) in 10 mM phosphate buffer (pH 7.4, 22 °C). C. Percent helicity calculated from CD spectra (θ_{220}) in 10 mM phosphate buffer, 20% ACN or 20 mM SDS buffer (**5d**,**e** not helical). D. IC_{50} = mean peptide concentration to inhibit 50% binding of fluorescent **1-FITC** (10 nM) to hDM2 (25 nM) measured by FP. $pIC_{50} \pm$ SEM values are reported in Fig. S1 (ESI†). Binding affinity (K_i) calculated from IC_{50} values. E. Heatmap indicating percent peptide intact after 2 h incubation with chymotrypsin (Chy), pepsin (Pep) or proteinase K (ProK) at 22 °C, pH 8 or 2 (Pep only), measured by LCMS. Arrows point to the respective cleavage sites as revealed by LCMS analysis of the cleaved fragments.

with a decafluorobiphenyl linker[23] that enhanced cell penetration of peptides.[23,30] However, is this linker an effective helix-inducing constraint? In the one report of helicity,[23] ($i \rightarrow i + 4$)-stapling of a 14-mer peptide with perfluorobiphenyl only modestly altered α-helicity. We created a Cys4-Cys11 ($i \rightarrow i + 7$)-crosslink with decafluorobenzyl, but the macrocycle (**5a**, Fig. 5A) had little helicity (Fig. 5B and C), weak hDM2 binding (Fig. 5D), and was degraded by proteases (Fig. 5E).

Towards a better ($i \rightarrow i + 7$) linker, we constructed new perfluorobiphenyl analogues **5b–e** that expanded ring size, altered D-, L-, α-methylated Cys, and altered the position of the connecting S–C bond. Increasing macrocycle size by two methylene units (**5b**) enhanced helicity, hDM2 binding, and protease resistance (Fig. 5). D- or α-methyl Cys substitution made positions 3–4 and 11–12 more protease resistant (Fig. 5E). Compounds **5d** and **5e** had unidentified CD curves (Fig. 5B), but increased hDM2 affinity *vs.* other perfluorobiphenyl analogues. Overall, perfluorination increased protease stability, but led to a ≥3-fold decrease in binding affinity for hDM2 *versus* **1**.

Hydrophobicity

Differences in hydrophobicity between compounds were compared by HPLC retention times (Fig. 6A), calculated octanol/water partition coefficients (clogP), and calculated total hydrophobic surface area (tHSA). HPLC retention time (Fig. 6A) varied considerably with cyclization linker (lactams eluting faster), correlating with both clogP over 9 log units (Fig. 6B and C) and calculated tHSA over 200 Å^2 (Fig. 6B and D). HPLC retention time correlated better with clogP (ChemDraw 20.0, R^2 = 0.84, Fig. 6C) than other calculations (*e.g.* AlogP, Fig. S3, ESI†). Using energy-minimized α-helical models (Maestro, Schrödinger), we estimated tHSA and total surface area for each peptide and found a significant correlation between tHSA and HPLC retention time (Fig. 6D).

Lactam bridges hardly altered surface area or volume relative to acyclic **1**, whereas hydrocarbon and perfluoroaryl-linked homocysteine staples conferred the greatest hydrophobicity in each series. As expected, hydrophobicity substantially increased (28–40%) with hydrophobic ($i \rightarrow i + 7$)-crosslinkers. Two α-methyl groups increased clogP by one long unit, but did not change tHSA much (0.5–4.5%) (Fig. 6B). Noticeably, perfluorobiphenyl analogues **5b** and **5c** had substantially different HPLC retention times despite similar clogP and tHSA, suggesting an impact of different geometries adjacent to the biphenyl ring. Outlier **3a** had intermediate tHSA contrasting with its high HPLC retention time and clogP.

Cell uptake

Cell uptake of the FITC-labelled peptides into HeLa cells was quantified by flow cytometry under serum-free conditions

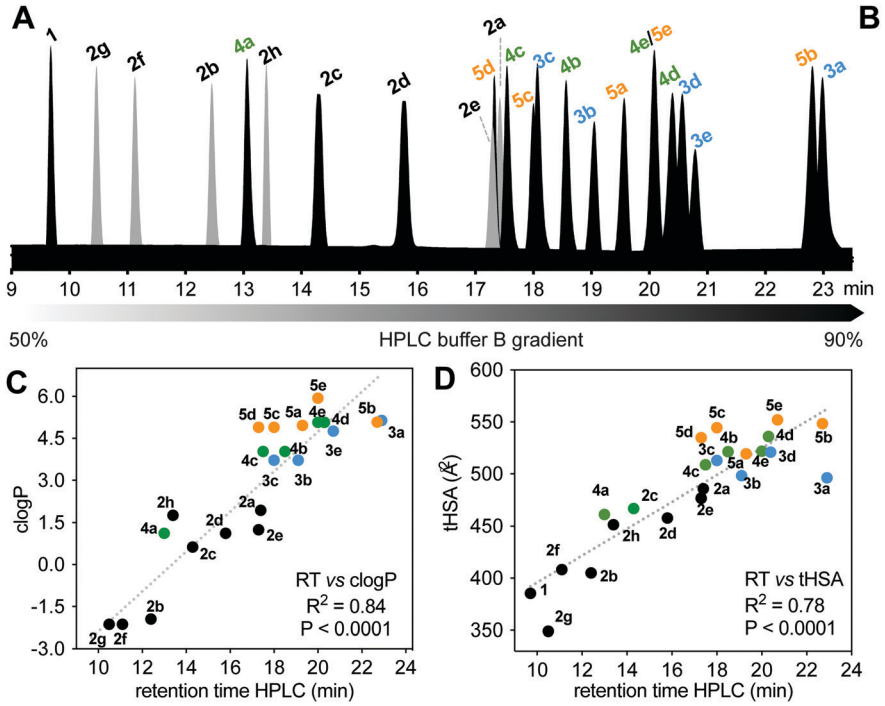

	Peptide	clogP	tHSA (Å²)	Total area (Å²)
Linear	1	-4.39	386	639
	1 (E5)	-3.57	390	661
(i→i+4) staples	2a	1.94	486	689
	2b	-1.95	405	646
	2c	0.63	467	690
	2d	1.12	458	730
	2e	1.25	477	772
	2f	-2.13	408	691
	2g	-2.13	349	596
	2h	1.76	452	656
Aliphatic (i→i+7) staples	3a	5.14	496	702
	3b	3.72	498	747
	3c	3.72	513	810
	3d	4.76	521	774
	3e	4.76	516	750
Aromatic (i→i+7) staples	4a	1.12	461	830
	4b	4.03	521	802
	4c	4.03	509	828
	4d	5.07	536	824
	4e	5.07	522	804
Perfluoro biphenyl (i→i+7) staples	5a	4.96	520	773
	5b	5.08	548	798
	5c	4.90	545	807
	5d	4.90	535	803
	5e	5.94	552	800

Fig. 6 Hydrophobicity of **1**, **2a–h**, **3a–e**, **4a–e**, **5a–e**. A. HPLC analysis showing retention time for each peptide using a C18 column (Phenomenex Luna), at 1 mL min^{-1} flow and 2.5 buffer B (0.1% TFA, 90% ACN) gradient per minute. B. Calculated parameters: logP (clogP), total hydrophobic surface area (tHSA) and total surface area for each peptide. C and D. Correlation between clogP (2D hydrophobicity) and HSA (3D hydrophobic surface area) calculated for each peptide *vs.* experimental HPLC retention.

(Fig. 7A), with cell-penetrating peptide TAT as control. The fluorescent label did not significantly change hydrophobicity relative to *N*-acetylated peptides, according to HPLC retention time (Fig. S4, ESI†). clogP and total hydrophobic surface area (tHSA) calculated for *N*-acetylated peptides was correlated with cell uptake (Fig. 7B and C). Only peptides with high hydrophobicity (clogP > 3.5, tHSA > 475 Å^2) entered HeLa cells (Fig. 7). Most FITC-labelled peptides were α-helical in membrane-simulating SDS buffer (Fig. S5, ESI†), but there was no overall correlation between helicity and cell uptake, even among peptides with high clogP values.

Of the ($i \rightarrow i + 4$)-series, only **2e**-FITC has substantially entered the cells, despite similar properties to **2a**-FITC that has only marginally more uptake than **1**-FITC. The shorter perfluorophenyl-stapled compound **2d**-FITC also exhibited moderate internalization despite its unruled structure and reduced lipophilicity, suggesting that the perfluorophenyl thioether promotes cell uptake. Lactam linkages were too polar to promote cell uptake, even when combined with a second hydrocarbon bridge (**2h**-FITC, clogP < 3.5; HSA < 475 Å^2). Of the ($i \rightarrow i + 7$)-series, cell uptake correlated somewhat with peptide hydrophobicity (R^2 = 0.55); aliphatic and non-fluorinated aromatic staples displaying comparable activity. The very hydrophobic perfluorobiphenyl compounds were the most internalized into HeLa cells, with **5b**-FITC the most cell uptaken peptide. α-Methylation stabilized helical structure, but surprisingly did not increase cell uptake.

Live cell confocal microscopy was used to visualize internalization of non-lytic FITC-labelled peptides (**2e**, **3a**, **3c**, **4c**, **5c**; see next section under cell lysis) into live HeLa cells, avoiding artefacts of cell fixation. All peptides (5 μM) exhibited significantly more cell uptake than cell-penetrating peptide TAT (Fig. 7D), in agreement with flow cytometry results (Fig. 7A). Peptides showed a punctate intracellular fluorescence distribution, typical of endocytosis and sequestration.[31] Similar experiments with lytic peptide **5b**-FITC showed even more peptide in the membrane and some endocytotic internalization early during incubation, followed by significant cell damage and cell death after 3 h (Fig. 7D). None of the stapling configurations studied here led to fast endosomal release to the cytosol in HeLa cells. We note that hydrocarbon-stapled peptides such as **3a** have been reported to reach the cytosol in sufficient amounts to activate p53-apoptotic pathways in other cancer cell lines.[19] One such peptide is ALRN-6924, a promising p53/hDM2 inhibitor peptide drug currently undergoing clinical trials.[32]

Cell lysis

Non-specific lysis of HeLa cells by the *N*-acetylated peptides (12 μM, 1 h, Fig. 8) was measured colorimetrically by lactate dehydrogenase (LDH) liberated from the cytosol. HeLa cells were used as they do not respond quickly to activation of the p53 pathway, and early onset of cell damage suggests non-specific membrane lysis induced by the peptides and not by triggering apoptosis. LDH release after 1 h (Fig. 8A) indicated that only the most hydrophobic peptides (**3a**, **5a**, **5b**, **5e**) promoted cell lysis (clogP ≥ 5, Fig. 8B) in a concentration-dependent manner (Fig. S6, ESI†). At lower concentrations (<6 μM), **3a** did not cause significant lysis, whereas **5b** was

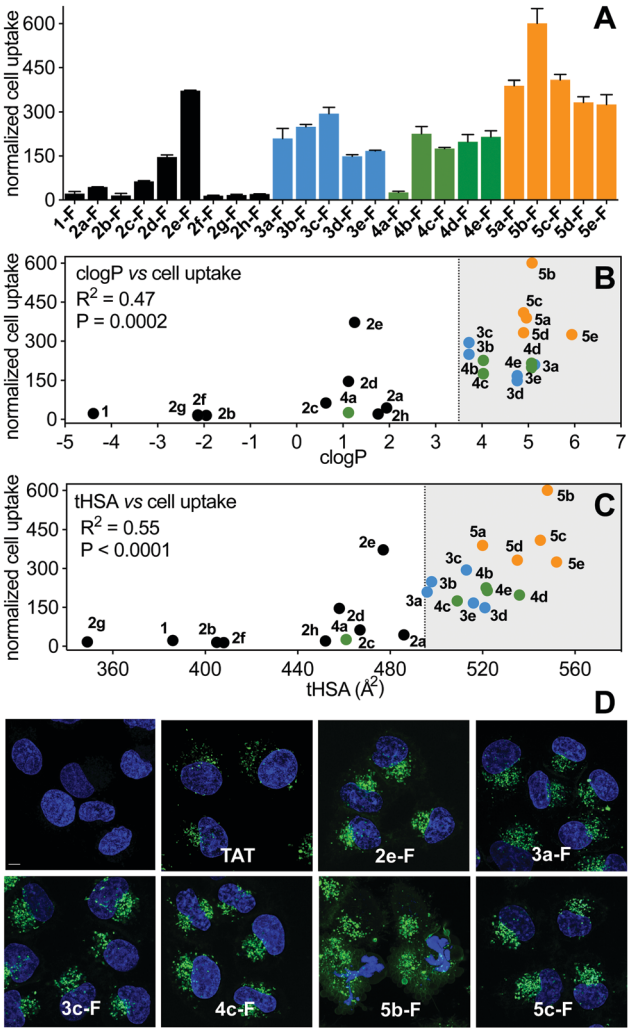

Fig. 7 A. Cell uptake of FITC-labelled peptides (5 μM) in HeLa cells measured by flow cytometry. Median fluorescence intensity measured after treatment with trypan blue (to eliminate membrane-bound peptide fluorescence) and normalized to TAT. Data = mean ± SEM. B and C. Correlation of cell uptake with clogP (B) or tHSA (C). D. Live confocal microscopy shows internalization of FITC-labelled peptides (5 μM) into HeLa cells after 3 h. Nuclei stained with Hoechst (blue), peptide green (FITC channel). Scale bar represents 5 μm.

cytotoxic even at 1 μM (Fig. S6, ESI†). Peptides **3c**, **4c** and **5c** with lower hydrophobicity (clogP 3.5–5), internalized into HeLa cells with no lysis even at 50 μM (Fig. S6, ESI†).

Discussion

We have systematically compared the impact of diverse helix-inducing cyclisation constraints on the structure, affinity (hDM2), proteolytic resistance and cell uptake properties of a 12-mer peptide inhibitor of oncogenic p53/hDM2). The linear sequence (**1**) has little α-helicity, is rapidly and completely degraded by proteases, and its sequence is not sufficiently hydrophobic or amphipathic to permeate cell membranes. Crosslinking two amino acid sidechains at (i, i + 4) or (i, i + 7)

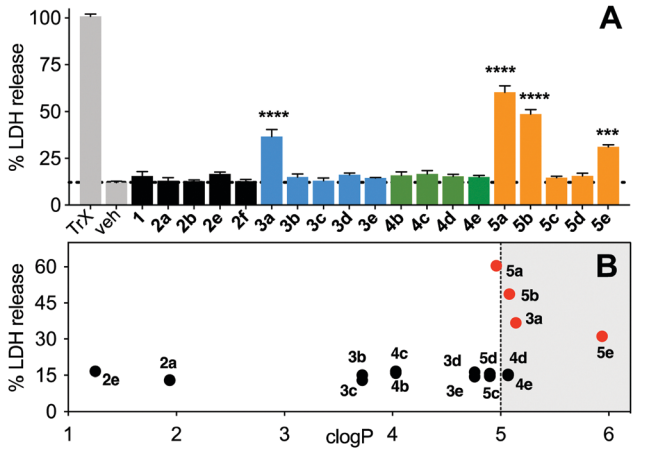

Fig. 8 A. LDH release after incubation of stapled peptides (12 μM) in HeLa cells for 1 h. Data = mean ± SEM. One-way ANOVA, *** (P < 0.001), **** (P < 0.0001). B. LDH release *versus* calculated hydrophobicity (clogP).

positions to constrain one- or two-turns of a helix, respectively, can be optimised to form macrocyclic components that can mitigate these problems.

The field of peptide stapling has expanded considerably over the last decade, with different chemical approaches to constrain peptides into helices. However, macrocyclization is limited by chemoselective reactions that work in solution with unprotected peptides (thiolation, click reaction) or are high-yielding conversions on solid-phase (RCM, lactamization). In particular, stapling across longer distances (i → i + 7) with retention of helicity can be more challenging, with fewer literature reports despite yielding the most clinically advanced stapled peptide to date (ALRN-6924).[32] Here, we used RCM, *S*-alkylation and *S*-arylation chemistry to insert diverse (i → i + 7)-crosslinkers into **1** and compared their properties to (i → i + 4)-crosslinkers.

Enhancing helicity of 1

All (i, i + 4) staples substantially increased α-helicity in water relative to **1** (Fig. 2). Maximum helicity in water for one (i → i + 4) staple was 60% (**2a** (hydrocarbon), **2f** (lactam)) and one (i → i + 7) staple was 70% (**3d**, **3e** (α-methyl octanyl thioether), while ≥90% helicity was achieved with two (i → i + 4) crosslinks (**2g**, **2h**). α-Methyl substitution increased helicity in aliphatic or aromatic thioether stapled compounds, particularly after the switch to D-Cys at positions 4 (**3e**, **4e**, **5e**), mirroring the strategy used to develop the (i → i + 7)-hydrocarbon[6a] in **3a**.

Solvent-exposed lactam staples showed greater hDM2 affinity

The N-terminus of p53 is intrinsically disordered but folds into an amphipathic helix upon binding to hDM2. A short sequence corresponding to this p53 region has negligible helicity and binds weakly to hDM2, but high affinity can be obtained by insertion of a helix-inducing constraint[33] that maintains residues corresponding to Phe19, Trp23, Leu26 of the p53 on the same helical face (Fig. 9). Surprisingly, we found no correlation between % helicity promoted by the various PDI-staples and

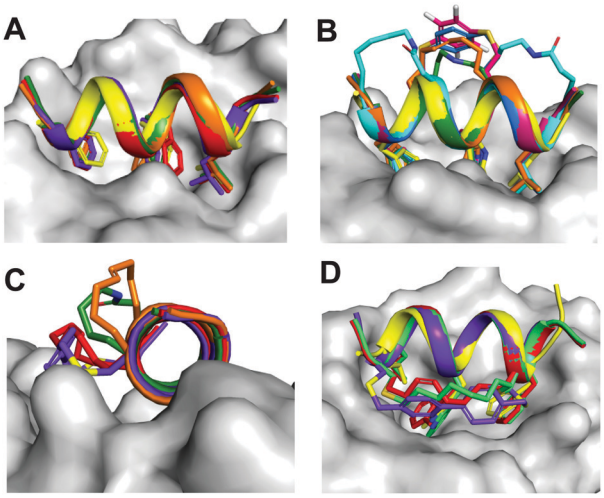

Fig. 9 Molecular modelling showing superimposition of stapled peptides bound to hDM2. A. Alignment of Phe3-Trp7-Leu10 at the same hDM2-binding site. B–D. The (*i*, *i* + 4)-crosslinkers of (**2a** (orange), **2b** (green), **2c** (blue), **2e** (magenta), **2f** (cyan) project into solvent, whereas (*i*, *i* + 7)-staples of **3a** (red), **3c** (green), **4c** (purple) face a hydrophobic pocket located at the boundary of the PPI interface.

peptide binding affinity for hDM2, indicating that the induced-fit for **1** is a powerful driver even without preorganized helicity in the peptide.

Molecular modelling was used to investigate conformational limitations to adopting the hDM2-binding helix in the presence of the crosslinking staples. The ($i \rightarrow i + 4$) crosslinkers project into solvent and so do not interfere with hDM2 interactions. However, ($i \rightarrow i + 7$) staples face a hydrophobic pocket at the hDM2 surface (Fig. 9). The small size of lactam bridges together with superior helix induction conferred the highest hDM2 affinity to peptides **2b** and **2f**, enabling them to project hydrophobic Phe3, Trp7 and Leu10 sidechains deep into hDM2 without steric interference from the stapled linker. For the ($i \rightarrow i + 7$) series, bulkier aromatic crosslinkers were less favourable than aliphatic linkers for hDM2 affinity, possibly due to unfavourable contacts with the rim of the hDM2 binding site. Such contacts were observed in the crystal structure of hDM2 bound to a ($i \rightarrow i + 7$) hydrocarbon-crosslinked p53 peptide,[34] and were proposed to assist binding. Controversially, we found here that hydrophilic ($i \rightarrow i + 4$) staples that did not interact with the hDM2 protein surface bound even more avidly.

Staples affect proteolytic resistance

Most proteases recognize an extended or β-strand like ligand conformation in their active sites.[27] Peptides constrained to, or flexible enough to adopt, that structure are cleaved faster than peptides constrained to helical or turn structures.[27d] Insertion of the crosslinking staples can slow peptide degradation, by reinforcing α-helical structure and reducing propensity to form an extended conformation recognized and processed by proteases, or by creating a protective shield that denies protease access to amino acid residues adjacent to the staple. All stapling constructs investigated here increased resistance to three common digestive proteases that rapidly cleave unstapled **1**. Whereas most staples conferred strong resistance to chymotrypsin, some left the peptide vulnerable to the action of proteinase K and pepsin, emphasizing the importance of measuring degradation against multiple proteases to gauge stability. Pepsin digestion is valuable for assessing peptide proteolysis in acidic environments such as found in the digestive tract.

Cysteine-linked peptides showed the lowest protection, allowing cleavage at positions inside and outside the cycle, but this was mitigated by a D-Cys (partially) or α-methyl substituent. Implementing both modifications led to thioether peptides with higher proteolytic resistance, comparable to hydrocarbon-stapled peptides with α-methyl substitution (**2a**, **3a** *vs.* **3e**, **4e**, **5e**). An unstapled analogue of peptide **2a** strongly resisted the action of proteinase K, implying that the α-methyl alkane residue *per se* offers strong proteolytic protection to the 12-mer peptide (Fig. S7, ESI†). Interestingly, lactam staples that contained no D- or α-substituted amino acids were exceptionally stable to degradation, suggesting a robust helical configuration that was protective. Moreover, single lactam or hydrocarbon ($i \rightarrow i + 4$)-stapling across positions 4–8 was sufficient to shelter the peptide bonds from the proteases, including blocking hydrolysis of residues located outside the macrocycle but held in a helical conformation. Similar protection was only observed in the ($i \rightarrow i + 7$)-series when α-methylation was also implemented. Double stapling (**2g**, **2h**) was not required to secure full proteolytic resistance to the 12-mer peptide, but this may be necessary for longer sequences.[35]

A hydrophobic balance for cell uptake without lysis

Unlike many studies of cell penetrating peptides, the sequence used here lacks positively charged amino acids. Indeed, incorporating Glu5 introduced a negative charge, yet the peptides still interacted with membranes and were taken up into cells, dictated primarily by the hydrophobic linker. Peptides with hydrophilic linkers (lactams, triazoles) did not internalize readily, regardless of how well they stabilized helical structure. Only chemical modifications that enlarged the solvent-exposed hydrophobic surface area of the molecule led to higher cell uptake, independently of helicity. α-Methyl substitution incrementally increased lipophilicity of the peptide, but it did not significantly increase the hydrophobic surface area and did not enhance cell uptake.

Overall, ($i \rightarrow i + 7$)-crosslinked peptides were more taken up into cells than ($i \rightarrow i + 4$)-counterparts because they considerably expanded the hydrophobic surface of the peptide. Of the ($i \rightarrow i + 4$) series, the increase in cell uptake was small but noticeable, with lactam $\ll$ hydrocarbon $<$ benzyl $\ll$ perfluorophenyl, a trend also observed for staples in a peptide that binds to estrogen receptor coactivator.[14] Perfluoro-phenyl analogue **2e** was an exception. Of the ($i \rightarrow i + 7$)-series, aliphatic and biphenyl crosslinkers gave comparable cell uptake, but perfluorination of the aromatic ring triggered greater entry. Compounds with greater hydrophobicity (clogP $>$ 5) led to cell lysis.

In summary, a compromise between helicity, protein affinity, protease resistance, hydrophobic surface area and cell membrane association are required in these kinds of peptides to achieve greater entry to cancer cells, not get trapped in endosomes, and interact strongly with target intracellular proteins without causing cell lysis.

Author contributions

A. D. A. synthesized peptides, measured CD spectra, protease stability and binding affinity. J. L. and K.-C. W. performed cell assays. H. N. H. calculated structural and biophysical properties. H. T. N. synthesized crosslinkers and α-methyl-cysteine units. D. P. F. obtained funding. A. D. A. and D. P. F. wrote the paper with input from all authors.

Conflicts of interest

The authors declare no conflicts of interest.

Acknowledgements

We thank ARC (DP180103244, DP160104442, CE200100012) and NHMRC (SPRF1117017, 1128908 1145372 and 2009551) for funding.

References

1 (*a*) D. E. Scott, A. R. Bayly, C. Abell and J. Skidmore, *Nat. Rev. Drug Discovery*, 2016, **15**, 533–550; (*b*) H. Lu, Q. Zhou, J. He, Z. Jiang, C. Peng, R. Tong and J. Shi, *Signal Transduction Targeted Ther.*, 2020, **5**, 213; (*c*) C. V. Dang, E. P. Reddy, K. M. Shokat and L. Soucek, *Nat. Rev. Cancer*, 2017, **17**, 502–508.

2 S. Jones and J. M. Thornton, *Proc. Natl. Acad. Sci. U. S. A.*, 1996, **93**, 13–20.

3 (*a*) N. E. Shepherd, G. Abbenante and D. P. Fairlie, *Angew. Chem., Int. Ed.*, 2004, **43**, 2687–2690; (*b*) N. E. Shepherd, H. N. Hoang, G. Abbenante and D. P. Fairlie, *J. Am. Chem. Soc.*, 2005, **127**, 2974–2983; (*c*) R. S. Harrison, N. E. Shepherd, H. N. Hoang, G. Ruiz-Gómez, T. A. Hill, R. W. Driver, V. S. Desai, P. R. Young, G. Abbenante and D. P. Fairlie, *Proc. Natl. Acad. Sci. U. S. A.*, 2010, **107**, 11686–11691.

4 V. Azzarito, K. Long, N. S. Murphy and A. J. Wilson, *Nat. Chem.*, 2013, **5**, 161–173.

5 (*a*) H. Wang, R. S. Dawber, P. Zhang, M. Walko, A. J. Wilson and X. Wang, *Chem. Sci.*, 2021, **12**, 5977–5993; (*b*) N. S. Robertson and D. R. Spring, *Molecules*, 2018, **23**, 959; (*c*) M. Pelay-Gimeno, A. Glas, O. Koch and T. N. Grossmann, *Angew. Chem., Int. Ed.*, 2015, **54**, 8896–8927.

6 (*a*) C. E. Schafmeister, J. Po and G. L. Verdine, *J. Am. Chem. Soc.*, 2000, **122**, 5891–5892; (*b*) L. D. Walensky and G. H. Bird, *J. Med. Chem.*, 2014, **57**, 6275–6288; (*c*) P. M. Cromm, J. Spiegel and T. N. Grossmann, *ACS Chem. Biol.*, 2015, **10**, 1362–1375.

7 D. P. Fairlie and A. Dantas de Araujo, *Biopolymers*, 2016, **106**, 843–852.

8 Y. H. Lau, P. de Andrade, S.-T. Quah, M. Rossmann, L. Laraia, N. Skold, T. J. Sum, P. J.-E. Rowling, T. L. Joseph, C. Verma, M. Hyvonen, L. S. Itzhaki, A. R. Venkitaraman, C. J. Brown, D. P. Lane and D. R. Spring, *Chem. Sci.*, 2014, **5**, 1804–1809.

9 Peptide stapling reviews: (*a*) L. McDougall and A. G. Jamieson, *eLS*, John Wiley & Sons, Ltd, 2022, **https://doi.org/10.1002/9780470015902.a002840**; (*b*) X. Li, S. Chen, W.-D. Zhang and H.-G. Hu, *Chem. Rev.*, 2020, **120**, 10079–10144; (*c*) M. Moiola, M. G. Memeo and P. Quadrelli, *Molecules*, 2019, **24**, 3654; (*d*) Y. H. Lau, P. de Andrade, Y. Wu and D. R. Spring, *Chem. Soc. Rev.*, 2014, **44**, 91–102.

10 G. H. Bird, E. Mazzola, K. Opoku-Nsiah, M. A. Lammert, M. Godes, D. S. Neuberg and L. D. Walensky, *Nat. Chem. Biol.*, 2016, **12**, 845–852.

11 A. D. Kalafatovic and E. Giralt, *Molecules*, 2017, **22**, 1929.

12 A. D. de Araujo, H. N. Hoang, W. M. Kok, F. Diness, P. Gupta, T. A. Hill, R. W. Driver, D. A. Price, S. Liras and D. P. Fairlie, *Angew. Chem., Int. Ed.*, 2014, **53**, 6965–6969.

13 H. N. Hoang, R. W. Driver, R. L. Beyer, T. A. Hill, A. D. de Araujo, F. Plisson, R. S. Harrison, L. Goedecke, N. E. Shepherd and D. P. Fairlie, *Angew. Chem., Int. Ed.*, 2016, **55**, 8275–8279.

14 Y. Tian, Y. Jiang, J. Li, D. Wang, H. Zhao and Z. Li, *ChemBioChem*, 2017, **18**, 2087–2093.

15 Y. Wang and D. H. Chou, *Angew. Chem., Int. Ed.*, 2015, **54**, 10931–10934.

16 A. Dantas de Araujo, S. R. Perry and D. P. Fairlie, *Org. Lett.*, 2018, **20**, 1453–1456.

17 B. Hu, D. M. Gilkes and J. Chen, *Cancer Res.*, 2007, **67**, 8810–8817.

18 G. Sanz, M. Singh, S. Peuget and G. Selivanova, *J. Mol. Cell Biol.*, 2019, **11**, 586–599.

19 Y. S. Chang, B. Graves, V. Guerlavais, C. Tovar, K. Packman, K. H. To, K. A. Olson, K. Kesavan, P. Gangurde, A. Mukherjee, T. Baker, K. Darlak, C. Elkin, Z. Filipovic, F. Z. Qureshi, H. Cai, P. Berry, E. Feyfant, X. E. Shi, J. Horstick, D. A. Annis, A. M. Manning, N. Fotouhi, H. Nash, L. T. Vassilev and T. K. Sawyer, *Proc. Natl. Acad. Sci. U. S. A.*, 2013, **110**, E3445–3454.

20 (*a*) K. Hu, H. Geng, Q. Zhang, Q. Liu, M. Xie, C. Sun, W. Li, H. Lin, F. Jiang, T. Wang, Y.-D. Wu and Z. Li, *Angew. Chem., Int. Ed.*, 2016, **55**, 8013–8017; (*b*) G. Philippe, Y.-H. Huang, O. Cheneval, N. Lawrence, Z. Zhang, D. P. Fairlie, D. J. Craik, A. D. de Araujo and S. T. Henriques, *J. Pept. Sci.*, 2016, **106**, 853–863; (*c*) G. Philippe, A. Mittermeier, N. Lawrence, Y.-H. Huang, N. D. Condon, A. Loewer, D. J. Craik and S. T. Henriques, *ACS Chem. Biol.*, 2021, **16**, 414–428; (*d*) P. G. Dougherty, J. Wen, X. Pan, A. Koley, J.-G. Ren, A. Sahni, R. Basu, H. Salim, G. Appiah Kubi, Z. Qian and D. Pei, *J. Med. Chem.*, 2019, **62**, 10098–10107; (*e*) Y. H. Lau, Y. Wu, M. Rossmann, B. X. Tan, P. de Andrade, Y. S. Tan,

C. Verma, G. J. McKenzie, A. R. Venkitaraman, M. Hyvönen and D. R. Spring, *Angew. Chem., Int. Ed.*, 2015, **54**, 15410–15413.

21 Z. Muppidi, X. Wang, J. Li, J. Chen and Q. Lin, *Chem. Commun.*, 2011, **47**, 9396–9398.

22 H. Jo, N. Meinhardt, Y. Wu, S. Kulkarni, X. Hu, K. E. Low, P. L. Davies, W. F. DeGrado and D. C. Greenbaum, *J. Am. Chem. Soc.*, 2012, **134**, 17704–17713.

23 A. M. Spokoyny, Y. Zou, J. J. Ling, H. Yu, Y.-S. Lin and B. L. Pentelute, *J. Am. Chem. Soc.*, 2013, **135**, 5946–5949.

24 S. J.-M. Verhoork, C. E. Jennings, N. Rozatian, J. Reeks, J. Meng, E. K. Corlett, F. Bunglawala, M. E.-M. Noble, A. G. Leach and C. R. Coxon, *Chem. – Eur. J.*, 2019, **25**, 177–182.

25 A. D. de Araujo, J. Lim, K. C. Wu, Y. Xiang, A. C. Good, R. Skerlj and D. P. Fairlie, *J. Med. Chem.*, 2018, **61**, 2962–2972.

26 (*a*) T. A. Hill, N. E. Shepherd, F. Diness and D. P. Fairlie, *Angew. Chem., Int. Ed.*, 2014, **53**, 13020–13041; (*b*) M. J. Kelso, R. L. Beyer, H. N. Hoang, A. S. Lakdawala, J. P. Snyder, W. P. Oliver, T. A. Robertson, T. G. Appleton and D. P. Fairlie, *J. Am. Chem. Soc.*, 2004, **126**, 4828–4842; (*c*) R. L. Beyer, H. N. Hoang, T. G. Appleton and D. P. Fairlie, *J. Am. Chem. Soc.*, 2004, **126**, 15096–15105.

27 (*a*) J. D.-A. Tyndall, T. Nall and D. P. Fairlie, *Chem. Rev.*, 2005, **105**, 973–1000; (*b*) P. K. Madala, J. D.-A. Tyndall, T. Nall and D. P. Fairlie, *Chem. Rev.*, 2010, **110**(6), PR1–PR31; (*c*) J. D.-A. Tyndall and D. P. Fairlie, *J. Mol. Recognit.*, 1999, **12**, 363–370; (*d*) D. P. Fairlie, J. D.-A. Tyndall, R. C. Reid, A. K. Wong, G. Abbenante, M. J. Scanlon, D. R. March, D. A. Bergman, C. L.-L. Chai and B. A. Burkett, *J. Med. Chem.*, 2000, **43**, 1271–1281.

28 (*a*) G. T. Perell, R. L. Staebell, M. Hairani, A. Cembran and W. C.-K. Pomerantz, *ChemBioChem*, 2017, **18**, 1836–1844; (*b*) G. Zhang, F. Barragan, K. Wilson, N. Levy, A. Herskovits, M. Sapozhnikov, Y. Rodríguez, L. Kelmendi, H. Alkasimi, H. Korsmo, M. Chowdhury and G. Gerona-Navarro, *Angew. Chem., Int. Ed.*, 2018, **57**, 17073–17078.

29 A. D. de Araujo, H. T. Nguyen and D. P. Fairlie, *ChemBioChem*, 2021, **22**, 1784–1789.

30 C. M. Fadzen, J. M. Wolfe, C.-F. Cho, E. A. Chiocca, S. E. Lawler and B. L. Pentelute, *J. Am. Chem. Soc.*, 2017, **139**, 15628–15631.

31 D. Y. Yoo, S. A. Barros, G. C. Brown, C. Rabot, D. Bar-Sagi and P. S. Arora, *J. Am. Chem. Soc.*, 2020, **142**, 14461–14471.

32 (*a*) M. N. Saleh, M. R. Patel, T. M. Bauer, S. Goel, G. S. Falchook, G. I. Shapiro, K. Y. Chung, J. R. Infante, R. M. Conry, G. Rabinowits, D. S. Hong, J. S. Wang, U. Steidl, G. Naik, V. Guerlavais, V. Vukovic, D. A. Annis, M. Aivado and F. Meric-Bernstam, *Clin. Cancer Res.*, 2021, **27**, 5236–5247; (*b*) C. Morrison, *Nat. Rev. Drug Discovery*, 2018, **17**, 531–533.

33 F. Bernal, A. F. Tyler, S. J. Korsmeyer, L. D. Walensky and G. L. Verdine, *J. Am. Chem. Soc.*, 2007, **129**, 2456–2457.

34 S. Baek, P. S. Kutchukian, G. L. Verdine, R. Huber, T. A. Holak, K. W. Lee and G. M. Popowicz, *J. Am. Chem. Soc.*, 2011, **134**, 103–106.

35 G. H. Bird, N. Madani, A. F. Perry, A. M. Princiotto, J. G. Supko, X. He, E. Gavathiotis, J. G. Sodroski and L. D. Walensky, *Proc. Natl. Acad. Sci. U. S. A.*, 2010, **107**, 14093–14098.